Emission and Nonradiative Decay of Nanodiamond NV Centers in a Low Refractive Index Environment

Faraz A. Inam,[†,‡,*] Michael D. W. Grogan,[¶,∥] Mathew Rollings,[¶] Torsten Gaebel,[†,‡] Jana M. Say,[†,‡] Carlo Bradac,[†,‡] Tim A. Birks,[¶] William J. Wadsworth,[¶] Stefania Castelletto,[†,‡] James R. Rabeau,[†,‡] and Michael. J. Steel[†]

[†]MQ Photonics Research Center and [‡]ARC Center of Excellence for Engineered Quantum Systems (EQuS), Department of Physics and Astronomy, Macquarie University, North Ryde, New South Wales 2109, Australia and [¶]Department of Physics, University of Bath, Claverton Down, Bath BA2 7AY, United Kingdom. [∥]Present address: Boston University, 8 Saint Mary's Street, Boston, Massachusetts 02215.

ABSTRACT The nitrogen vacancy (NV) center is the most widely studied single optical defect in diamond with great potential for applications in quantum technologies. Development of practical single-photon devices requires an understanding of the emission under a range of conditions and environments. In this work, we study the properties of a single NV center in nanodiamonds embedded in an air-like silica aerogel environment which provides a new domain for probing the emission behavior of NV centers in nanoscale environments. In this arrangement, the emission rate is governed primarily by the diamond crystal lattice with negligible contribution from the surrounding environment. This is in contrast to the conventional approach of studying nanodiamonds on a glass coverslip. We observe an increase in the mean lifetime due to the absence of a dielectric interface near the emitting dipoles and a distribution arising from the irregularities in the nanodiamond geometry. Our approach results in the estimation of the mean quantum efficiency (~0.7) of the nanodiamond NV emitters.

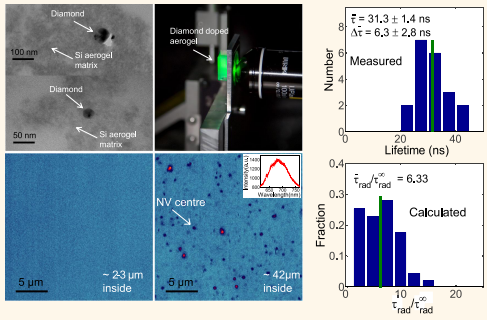

KEYWORDS: single-photon source · spontaneous emission rate · aerogel environment · single center emission · diamond NV center · quantum efficiency

The long-term development of several quantum technologies including quantum noise-limited measurement and computation are conditional on the development of bright on-demand sources of single photons.[1−5] The diamond nitrogen vacancy (NV) center is a strong candidate in this regard owing to its room-temperature photostability and high quantum efficiency.[6−8] However, its broad emission, moderate emission lifetime in bulk diamond of 12 ns, and low intrinsic photon capture factor pose problems. NV centers are generally believed to have a relatively high quantum efficiency,[8−11] so the radiative decay strongly influences the excited-state lifetime, and a variety of approaches to manipulate the local electromagnetic environment have been successfully employed to modify the spontaneous emission of these centers. Some methods couple the dipole emission to a strongly localized mode of a high-Q resonator such as a pure diamond ring resonator,[12] a microsphere,[13,14] a microdisk,[15] or a photonic crystal cavity.[16−19] Others exploit the large broad-band electromagnetic field enhancement associated with surface plasmons to achieve a significant enhancement in the overall emission rate.[11,20,21] Though this center has been widely studied in the past decade and significant enhancements in emission rate and capture factors have been achieved, the understanding of its spontaneous emission under the influence of the local electromagnetic nanoenvironment is still far from complete.

An important quantity in this context is the quantum efficiency

$$\eta = \frac{k_{\mathrm{rad}}^{\infty}}{k_{\mathrm{nr}} + k_{\mathrm{rad}}^{\infty}} \qquad (1)$$

where k_{nr} is the nonradiative decay rate and $k_{\mathrm{rad}}^{\infty}$ is the radiative decay rate in bulk

* Address correspondence to faraz.inam@mq.edu.au.

Received for review September 12, 2012 and accepted April 15, 2013.

Published online April 15, 2013
10.1021/nn304202g

diamond.[22,23] Thus η provides a normalized measure of the decay by nonradiative channels. (We discuss this definition in greater detail below in the section Quantum Efficiency). Recently, we found that, for the case of NV centers in nanodiamonds on a glass substrate, the observed decay rate is significantly faster than expected from calculations based on the literature value of the bulk diamond NV decay rate. These calculations assumed (as is typical in the literature) a near unity quantum efficiency for the NV emission, following the understanding of emission in bulk diamond.[24,25] In fact, the quantum efficiency of NV centers has been reported across the range of 0.7−0.99[8−11] and can be influenced by a number of effects such as intersystem crossing, phonon−electron coupling, spectral diffusion, surface proximity, and charge state. Even in the absence of strongly resonant electromagnetic structures, the influence on the emission rate from the electromagnetic local density of states (LDOS) is quite complicated. For example, the embedding of the NV center inside the nanodiamond and the random orientation of the NV dipole compared to the substrate−air interface both play significant roles:[24] the former tends to suppress the radiative emission due to a reduction in the local electric field inside the nanodiamond, while the latter broadens the observed distribution of rates due to the different coupling for emission parallel and perpendicular to the interface. These factors and the discrepancy in observed and predicted decay rates assuming unit quantum efficiency provoke the study of emission using strategies that can isolate the influences on both the mean value and statistical distribution of the decay rate.

In this work, we provide a novel approach for simplifying this problem to obtain a deeper understanding of the spontaneous emission of diamond NV centers. We introduce a new host environment to try to isolate the mechanisms influencing the spontaneous emission and total decay rates and to quantify the quantum efficiency. An ideal scenario would be to place the nanodiamonds containing single NV centers in an environment of refractive index as close as possible to unity ($n \sim 1$). The interface and orientation effects should then be largely removed. Since nanodiamonds on the order of 50 nm are difficult to trap using optical tweezers, obtaining a pure air environment is very challenging.[26] As a much simpler approach, we placed our diamonds inside silica aerogel materials (refer to Materials and Methods), in an environment with an average refractive index ($n \sim 1.05$).[27−29] Thus to the furthest extent possible, we remove the substrate altogether. By comparing measured and theoretical rates for two environments—glass coverslip and aerogel—we obtain a measure of the nonradiative emission of NV centers in both bulk diamond and nanodiamond (in this case, high-pressure high-temperature (HPHT) nanodiamonds). We thus obtain an estimate of the average quantum efficiency associated with the single NV centers. We note that a recent work on the direct synthesis of novel diamond aerogel structures studied ensemble emission from 100 and 5 nm diamond grains distributed through the aerogel lattice, for which a component of the emission spectrum was due to the NV center.[30] Our contrasting analysis of single center emission is therefore two-fold relevant. From the materials perspective, we prove the feasibility of integrating good quality nanodiamonds in aerogel such that their single center emission properties are preserved and not adversely affected by additional background fluorescence from the synthesis procedure. Further, our work allows the separation of substrate interface effects and their interaction with the NV dipole orientation from effects associated with the intrinsic local environment of the nanodiamond itself.

RESULTS AND DISCUSSION

In this section, we first summarize the relevant theory of spontaneous emission specific to the diamond NV center. We then assess the emission rates both experimentally and theoretically for two distinct systems (nanodiamonds on coverslip and inside silica aerogel) and extract values for the quantum efficiency.

Emission Rate Studies. A single center decaying by spontaneous emission is commonly considered as a radiating dipole. The spontaneous emission lifetime is strongly influenced by the spectral density of field-weighted photon decay channels, that is, the local density of electromagnetic states available to the emitted photons and the orientation of the dipole relative to the electric field in each mode.[31] Aside from the highly engineered resonant structures mentioned in the introduction, nanodiamond NV centers are typically characterized by placing them on a glass coverslip.[6,32,33] Emission from NV centers in this geometry has traditionally been treated using a simple picture that posits half the photon emission into air and half into the coverslip substrate. Using the fact that the emission rate in a homogeneous environment scales linearly with the refractive index, n, the net emission rate is then predicted to be

$$\Gamma = \frac{\Gamma_b}{2}\left(\frac{1}{n_d} + \frac{n_s}{n_d}\right) \tag{2}$$

where $\Gamma_b = 1/\tau_b$ is the lifetime in bulk diamond, and $n_d \approx 2.4$ and $n_s \approx 1.45$ are the refractive indices of diamond and the coverslip, respectively. This equation yields an average lifetime $\tau = 1/\Gamma \approx 22$ ns, which is indeed in agreement with experiments using nanodiamonds with size in the range of 50−100 nm.[24,32] The distribution in lifetimes with a width around 6 ns[24] is attributed to the random orientation of the dipole with respect to the dielectric interface of the coverslip combined with the polarization dependence of dipole emission at a surface.[6,24,34−36]

As we have discussed previously,[24] however, despite the apparent agreement with experimental lifetimes, this picture is incomplete, in terms of both purely electromagnetic influences as well as the other non-electromagnetic effects. To start, the emission rate also depends on the proximity of the dipole (within the host nanodiamond) to the interface.[35] In this case of dipoles radiating near an interface, the rate is governed by the interference between the directly emitted waves and those reflected from the surface and therefore is sensitive to the dipole polarization and separation relative to the dielectric interface.[35,36] Indeed, for nanodiamonds of size 5−10 nm, where the dipoles emit close to the interface, an average lifetime as low as 17 ns has been observed.[6] More importantly, the simple model of emission in two half-spaces neglects the critical fact that the NV dipoles are trapped inside a high-index diamond matrix of subwavelength scale. It is well-known that for emitters embedded in nanoparticles much smaller than the emission wavelength, λ, the emission rate is expected to be highly suppressed compared to the rate in a bulk crystal of the same material due to the Lorenz−Lorentz reduction in the local electric field.[25,37,38] According to the analytic results of Chew[37] for the spontaneous emission rate of a dipole inside a subwavelength sphere ($k_a \ll \lambda$) emitting in air, the emission rate is independent of the dipole location and polarization within the sphere and goes as

$$\Gamma = \Gamma^{\infty}\frac{1}{\sqrt{\varepsilon}}\left(\frac{3}{\varepsilon+2}\right)^2 \approx 0.062 \qquad (3)$$

where $\varepsilon = n^2$ and Γ^{∞} is the rate corresponding to a uniform medium density of states in a macroscopic piece of the same material. A large suppression in the emission rate and a corresponding increase in the lifetime is associated with a mesoscopic local-field or Lorenz−Lorentz effect, the electric field within the nanodiamond being strongly reduced by a factor of $3/(\varepsilon + 2)$ compared to the external field and approximately constant across the sphere. This corresponds to a reduction in the local density of states (LDOS) by an equivalent factor of $(3/(\varepsilon + 2))^2$.

These issues continue to play a role when the substrate is added, as discussed in detail in our previous work.[24] There, we considered single NV centers embedded in nanodiamond crystals with an average size of 54 nm, with the diamond crystals dispersed on a coverslip and opal photonic crystal surfaces. We measured the effect of the substrate surface topology on the emission rate and calculated the expected emission rate using both rigorous finite-difference time-domain (FDTD) simulations and a semianalytic approach assuming a negligible contribution from the nonradiative decay.[24] While the effect of changing the substrate was modest due to the nonresonant geometry, with the assumption of unit quantum efficiency, a discrepancy of about a factor of 4 emerged between the measured decay rate and both calculations of the radiative decay (the two calculations themselves being in close agreement). FDTD studies on a range of nanodiamond shapes (cubes, cuboids, pyramids, *etc.*) resting on a coverslip indicate that nonspherical nanodiamonds alter the mean and width of the radiative lifetime distribution but not nearly enough to account for the difference in the calculated and measured rates.[24] The discrepancy suggests that the total decay rate is strongly affected by nonradiative pathways. These could include transitions to and from the NV^- metastable state and vibronic side-bands,[7] quenching due to the presence of some other defects *via* phonon-assisted Coulomb coupling,[39] graphite phases, dislocations, residual stress,[40] surface chemistry, or spectral diffusion due to electron−phonon coupling. Many of these phenomena are intrinsic to the NV center emission within the diamond crystals. For example, nonradiative transitions between the NV^- excited and the metastable states are known to occur at rates similar to the radiative decay.[7] Further, in the nanoscale regime, the surface chemistry around the diamond crystals may have some contribution to the emission and decay rate; that is, a graphite shell surrounding the diamond crystals is known to quench photon emission.[41] Moreover, the phonon side-band spectrum of the NV emission can be significantly modified by changing the substrate from glass to silica on silicon at cryogenic temperatures.[42] It is therefore imperative to develop methods for determining the quantum efficiency. In the following sections, we assess emission rates both theoretically and experimentally for two distinct systems and extract values for the quantum efficiency.

Nanodiamond-Doped Silica Aerogel. Silica aerogels are lightweight, low density, and almost transparent pieces of glass[27,43,44] (see Materials and Methods section). The dimensions of the aerogel structure typically range from 1 to 5 nm for the glass elements and ~50 nm for the air-filled pores. Given the scale of these pores, various nanoparticles of comparable scale have previously been trapped as dopants.[44] We fabricated nanodiamond-doped aerogels using the "two-step" process, previously described for doping with gold nanoparticles[29] (refer to Materials and Methods). Following the aerogel preparation, we performed transmission electron microscopy (Philips CM10 transmission electron microscope with Olympus SIS megaview G2 digital camera unit) on the samples (Figure 1a). Isolated diamond crystals of varying size and geometry were found embedded inside the silica aerogel matrix. We performed confocal fluorescence imaging of the nanodiamonds embedded in the aerogel and nanodiamonds from the same source resting on a coverslip. In the aerogel configuration, the sample was attached to the surface of a coverslip and the laser was focused

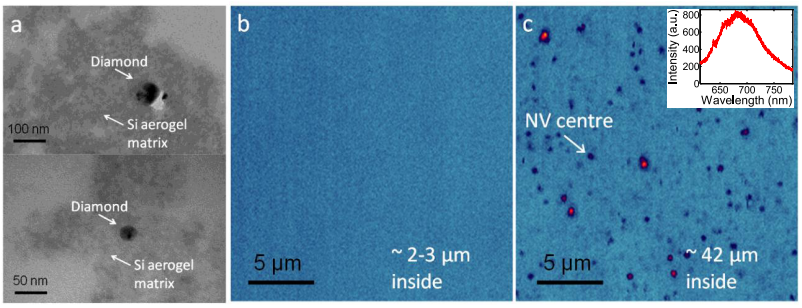

Figure 1. (a) TEM images showing isolated diamond crystals embedded inside the silica aerogel matrix. (b,c) Confocal images of different focal planes inside the aerogel sample. Most of the nanodiamond crystals were found at depths greater than 40 μm inside the aerogel surface (c). Inset: fluorescence spectrum of a single NV center inside the aerogel.

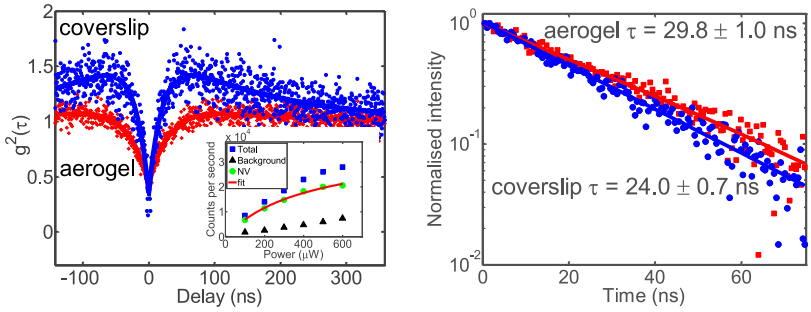

Figure 2. (a) Second-order autocorrelation curves $g^{(2)}(\tau)$ for single NV centers on coverslip and inside aerogel. (b) Time-resolved normalized fluorescence decay. Inset: saturation of a single NV center inside aerogel; total count rate C (blue squares), background (black triangles), background-subtracted counts (green dots). The red curve is a fit to the saturation model $C = C_{sat}P/(P + P_{sat})$, where P is the excitation power. The fitted saturation intensity counts $C_{sat} = (3.65 \pm 0.2) \times 10^4$ counts s^{-1} and saturation power $P_{sat} = 430 \pm 20$ μW.

from the other surface. Confocal scan images showed that most of the nanodiamonds are embedded deep inside the aerogel with almost zero fluorescence collected from planes near the surface (Figure 1b). To remove the contribution on the emission rate from the coverslip glass interface touching the aerogel surface, NV fluorescence was collected from planes ~40−90 μm inside the aerogel (Figure 1c). The collected photon counts for the case of NV centers inside the aerogel lattice were 2−3 times less than that measured for the case of diamonds on a coverslip as a result of scattering of both the excitation laser power and the emitted NV photons by the random silica structure comprising the aerogel volume.[27,28]

Lifetime Studies. For both coverslip and aerogel samples, fluorescence measurements were performed on the nanodiamond NV centers (refer to Materials and Methods). Crystals hosting single centers were identified using measurement of the second-order intensity correlation function $g^{(2)}(\tau)$, and only those with $g^{(2)}(0) < 0.5$ were studied further (Figure 2a). Based on our previous characterizations, less than 1% of nanodiamonds used in these experiments were expected to contain single NV centers.[45] In this case, we located $N_{cover} = 28$ single centers on the coverslip and $N_{aero} = 20$ single centers inside the aerogel sample. The measured spectrum from these single centers inside the aerogel corresponds to that of a NV (Figure 1c, inset). For these single centers, the excited-state NV^- lifetime τ was determined using time-resolved fluorescence measurements with pulsed 532 nm laser excitation and collection of the NV emission above 650 nm[46] (Figure 2b). This is important since the actual state of NV at 532 nm is a superposition of the NV^0 and NV^- charge states,[46] which possess different lifetimes (20 and 12 ns in bulk diamond, respectively). The zero phonon line (ZPL) of NV^- is at 638 nm, and typically, the phonon side-band is detected above 650 nm by filtering between 660 and 800 nm, while NV^0 has a ZPL at 575 nm and is detected typically between 575 and 630 nm.[46] In this work, we collect above 650 nm, and therefore we measure only the NV^- lifetime and quantum efficiency.

The distributions in measured lifetime for the two cases of coverslip and aerogel are shown in Figure 3. The mean lifetime for the diamonds on a coverslip was $\tau = 22.9 \pm 1.6$ ns and for the diamonds inside aerogel was $\tau = 31.3 \pm 1.4$ ns (uncertainties are the standard deviation of the mean). Figure 3 also shows the width (standard deviation) of the lifetime distribution along with the corresponding uncertainties based on variance of the variance. The change in NV center environment from the coverslip surface to inside the aerogel produced a mean lifetime increase of $\Delta\tau = 8.4 \pm 3$ ns, which is an increase of 37 ± 16%. We used the Kolmogorov−Smirnov test[47] to quantify the

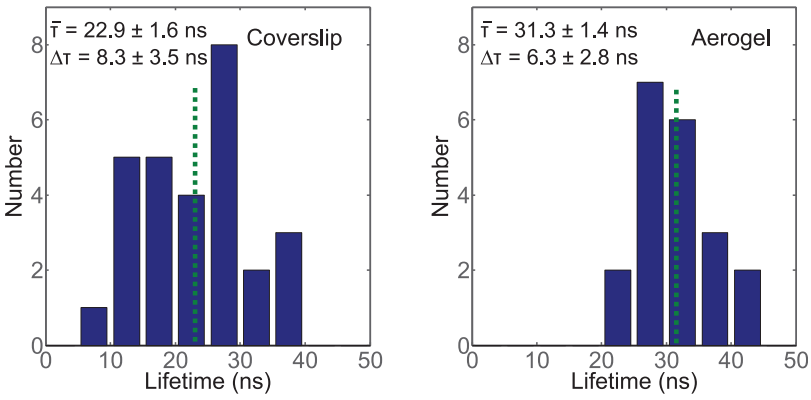

Figure 3. Experimental distribution of the NV center lifetime (a) on a coverslip and (b) inside aerogel. Dotted lines denote the mean value. The quoted values are the mean lifetime $\bar{\tau}$ and the standard deviation $\Delta\tau$.

difference in the two distributions. The null probability for the two sample distributions to be derived from the same underlying distribution was below 1%.

While the mean lifetime increases, there is a reduction in the relative distribution width $\Delta\tau/\tau$ from 0.36 ± 0.18 to 0.20 ± 0.10. A reduction in the relative width is expected because the aerogel configuration removes the spread in the decay rates arising as a result of varying dipole polarization and separation relative to the dielectric air/glass interface for the coverslip configuration (refer to Emission Rate Studies). However, the remaining width that is present in the aerogel distribution can be seen as a measure of the spread in lifetimes due to intrinsic properties of the nanodiamonds: shape, size, and internal variation such as strain or chemical variability.

Emission Rate Calculations. Although spontaneous emission is a quantum process, one can calculate the radiative emission rate relative to a reference system using classical electromagnetic calculations where the contribution of the environment is expressed through the local density of states (LDOS). In this work, we calculated the radiative decay rates of the nanodiamond NV centers on the coverslip or aerogel relative to the decay rate in bulk diamond using 3D FDTD simulation[48,49] (refer to Materials and Methods). The specific geometries we studied were a single nanodiamond crystal of average measured size of 54 nm (n_d = 2.416) on a glass coverslip (n = 1.45)[24] and a single nanodiamond embedded in the aerogel medium. Previous work has demonstrated that the aerogel structure can be regarded as a complex random network of sheets of silica spheres with pores of ~50 nm.[28,43] These studies show that embedded particles of 50 nm tend to occupy the pore sites, therefore, nanodiamonds of 50 nm can be simulated in the same way. Specifically, we modeled the nanodiamonds in the aerogel environment in two ways: first, a nanodiamond is embedded in a uniform material of average index n = 1.05[28] (a structure which is described analytically by the theory of Chew[37]); second, a nanodiamond inside a silica shell (n = 1.46) with a width of 5 nm surrounded by air is taken as an approximate model of the nearby environment within a pore.[28,43] As nanodiamonds have rather irregular shapes, and as the shape of the nanodiamond can influence the distribution width quite strongly,[24,50] we performed calculations for three representative nanodiamond forms: a sphere, a trapezoid, and a cube. Since our actual diamond crystals are known to be irregular in shape (as observed using SEM,[24] AFM,[45] and TEM microscopy techniques), we expect the observed behavior to lie within the range of distributions, with the trapezoid likely being the best representative (we discuss this further in a moment). For an isolated subwavelength sphere, it is well-known that the emission rate is very weakly dependent on both polarization and dipole location within the sphere, and we indeed calculate a very narrow distribution[37] (top row in Figure 4). The cube (bottom row) shows a significantly broader distribution than the sphere since, for that case, parallel and perpendicularly aligned dipoles lying close to one of the faces see quite distinct electromagnetic environments. The sharpness of the cube edges induces sharp changes in the electric field patterns and therefore a broader distribution of the emission rate.[24] Also, the sharp corners produce large electric fields around it, giving rise to an increase in the power radiated (*i.e.*, higher decay rates) by nearby dipoles. Hence, for the cube, the mean radiative lifetime is smaller compared to the sphere case. For the trapezoid (middle row in Figure 4), there is a reduction in the sharpness of some corners and the distinction between parallel and perpendicular orientation is intermediate but closer to the cubic case, as are the lifetime distribution widths. In our earlier study,[24] we examined the emission rate dependence for a range of nanodiamond shapes on a substrate and found that, while the sphere and cube gave extremal values due to the reasons discussed above (and as noted in ref 50), other convex structures including octahedra and ellipsoids showed surprisingly little dependence in either mean rates or distribution widths. Hence we expect that low symmetry structures

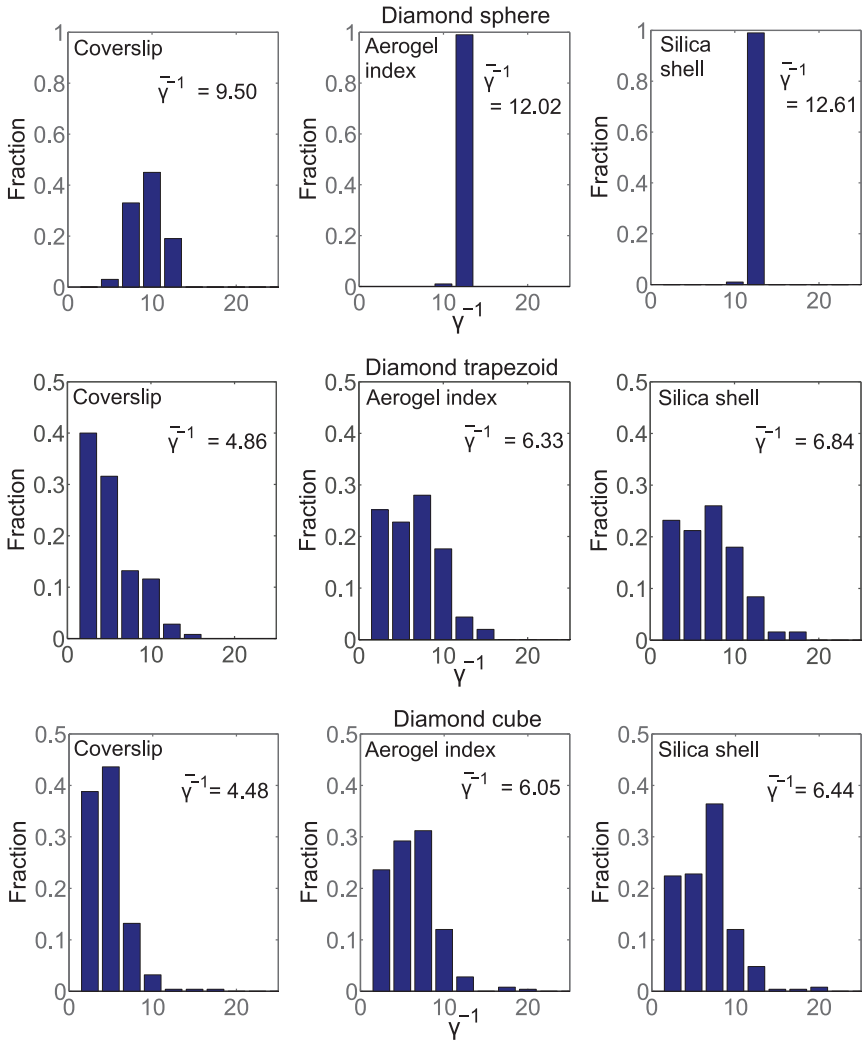

Figure 4. Normalized radiative lifetime γ^{-1} distributions using our FDTD calculation method for the cases of NV emission inside spherical (top row), trapezoidal (middle row), and cubic diamond crystals (bottom row) of size 54 nm for the configurations of diamond crystals placed on a coverslip (left column), inside a medium of aerogel index (center), and enclosed in a silica shell of 5 nm (right). Quoted values are the mean normalized radiative lifetimes for the respective cases; these compare with a calculated value of γ^{-1} = 14.5 for a diamond sphere in air.

like the trapezoid should be fairly insensitive to the exact shape[24] and a reasonable model for the irregular forms of real nanodiamonds. Note that the relative change in the radiative emission rates (around 25 to 40%) between the coverslip and the aerogel configuration is similar for all of the considered geometries of the diamond crystal.

Figure 4 also shows that, for each diamond shape, the difference between the two aerogel calculations (uniform index and silica shell) is about a factor of 3−4 smaller than that between the aerogel and coverslip configurations, suggesting that the random porous structure of tiny aerogel silica particles (∼1−5 nm) around the diamond crystal would not greatly alter the measured lifetimes. Therefore, given the fact that the real silica glass structure around the diamond crystal is much more random than a simplified 5 nm silica shell and that the influence of this randomness on the emission rate is relatively much smaller compared to that from the air/glass interface at the coverslip surface, in the remaining part of this paper, we take the uniform index model to represent the aerogel configuration. In considering the uncertainty in the predicted measured rates, the large number of simulations performed makes the statistical error in the calculated mean rate relatively small, *for the given diamond configuration in each set of FDTD calculations*. More important in estimating the genuine uncertainty is that the real diamonds have more complex forms than the ideal shapes of the diamonds in our FDTD calculations and also have a significant spread in size. To estimate the effect of the shape variation, we note from Figure 4 that the difference in the mean rates between the trapezoid form (middle row) and cube form (bottom row) is around 10%, comparable to the difference between the silica shell and uniform aerogel models (center and right columns, respectively). Recent calculations of emission rates in diamond spheres suggest a similar

TABLE 1. Measured and Calculated Radiative Properties for Different Environments[a]

NV environment	radiative enhancement γ_i (trapezoid calculation)	measured lifetime τ (ns)	total lifetime enhancement β	mean quantum efficiency $\bar{\eta}$	mean quantum efficiency $\bar{\eta}^{nano}$
bulk diamond	1	11.6	1	0.7−1.0	0.7[9]
nanodiamond on coverslip	0.21 ± 0.03	22.9 ± 1.6	1.97 ± 0.14	0.62 ± 0.14	0.66 ± 0.07
nanodiamond in aerogel	0.16 ± 0.02	31.3 ± 1.4	2.7 ± 0.12	0.75 ± 0.08	0.73 ± 0.05

[a] The average index model is considered to correspond to the aerogel configuration. The range of bulk diamond quantum efficiency values is based on refs 8−10, and 14.

uncertainty due to the size variation of 10%.[56] Combining these statistical contributions, we obtain a net uncertainty of ≈15% as a reasonable estimate. For comparison between the observed lifetimes and emission rate calculations, the measured average lifetimes and corresponding radiative enhancement for the different configurations of coverslip and aerogel are presented in Table 1. Here, the calculated values correspond to the trapezoidal geometry for the diamond crystals, and the average index scheme is taken as representative for the aerogel configuration [refer to Figure 4 (middle row, middle column)].

Quantum Efficiency. The quantum efficiency was defined earlier as $\eta = k_{rad}^{\infty}/(k_{nr} + k_{rad}^{\infty}) = (1 + \gamma_{nr})^{-1}$.[22,23] For convenience, we have now introduced the normalized nonradiative decay rate $\gamma_{nr} = k_{nr}/k_{rad}^{\infty}$. This definition of η allows us to separately identify the modification of the radiative decay rates due to the nanodiamond structure and its external environment and the nonradiative part associated with many possible quantum decay processes. The radiative environmental changes are essentially classical phenomena which are independent of the intrinsic quantum properties represented by γ_{nr}. We can now write the total decay rate k_i for nanodiamonds placed in geometry i as

$$\frac{1}{\tau_i} \equiv k_i = k_{rad}^{\infty}\gamma_i + k_{nr} = k_{rad}^{\infty}(\gamma_i + \gamma_{nr}) \qquad (4)$$

where τ_i is the excited-state lifetime, which serves to define γ_i as the radiative enhancement factor associated with the local electromagnetic environment. For emission in the reference bulk material, $\gamma_i = 1$. For a particular geometry i, we also define the enhancement factor of the total lifetime $\beta_i = \tau_i/\tau^{\infty} = k^{\infty}/k_i$, where $\tau^{\infty} = 1/k^{\infty} = [k_{rad}^{\infty}(1 + \gamma_{nr})]^{-1}$ is the center total lifetime in bulk diamond.

At this point, we must make an assumption about the relation between the nonradiative decay in bulk diamond and the nanodiamonds. If we consider that the dominant nonradiative pathways in NV centers can be attributed to the intersystem crossing and/or to photoionization induced by nearby charges, then a plausible assumption is that the nonradiative decay rates in bulk and nanosized diamond are similar. This assumption is supported by recent results showing that the dominant spectral diffusion in NV in nanodiamonds and in bulk diamond can be attributed to charge traps and photoconversion of NV^- to NV^0.[51,52] In this case, we obtain a simple expression from eqs 1 and 4 for the common quantum efficiency of

$$\eta = \frac{1 - 1/\beta_i}{1 - \gamma_i} \qquad (5)$$

This allows us to make some new observations and identify certain constraints on the quantum efficiency for the NV center in nanodiamonds, as there is a considerable discrepancy in the inferred NV center bulk diamond quantum efficiency, with reported values ranging from 0.7 to 1.0.[8−10,14] Table 1 summarizes the expected total lifetime enhancement factor β_i and radiative enhancement γ_i. From the two sets of measured and calculated data, we can use eq 5 to extract the value of the quantum efficiency that reconciles the measured decay rates and calculated emission rates, finding $\bar{\eta} = 0.75 \pm 0.08$ and $\bar{\eta} = 0.62 \pm 0.14$ for the aerogel and coverslip, respectively.

Note that as we do not have any knowledge of the individual nanoenvironment (diamond shape, size, dipole orientation) for each center, these quantum efficiency values are estimates of the mean value for the measured distribution (indicated by the overbar on η). The error limits for $\bar{\eta}$ estimate the statistical uncertainty in the two mean values and are not a measure of the distribution of quantum efficiencies present in the sample. We return to this below in the section on Quantum Efficiency Distribution.

The error quoted for the mean quantum efficiencies was estimated by propagation of the statistical errors in the measured lifetimes and calculated radiative enhancement factors, followed by application of the method of *expanded uncertainties*.[53] This attempts to account for the fact that the quantum efficiency η in eq 5, being a function of two strongly correlated variables (β, γ), should not be expected to follow a normal statistical distribution. The lifetime enhancement β is obtained from the measured lifetimes having a roughly normal statistical distribution. The radiative enhancement γ, a calculated quantity, has a complex distribution of values dependent on the different calculation parameters, such as the variations of diamond shape, environment variation, dipole location and orientation, and crystal size variation.

Considering the above scenario, the final distribution of the quantum efficiency is not known and is

unlikely to be Gaussian. Therefore, one standard deviation may not encompass the large fraction of the values expected from the quantum efficiency. We have therefore used the technique of *expanded uncertainties*[53] to obtain error limits (refer to Table 1) that would correspond to three standard deviations if the distribution had been Gaussian.

However, the assumption of unchanged quantum efficiency between the bulk and nanodiamond centers might well be questioned. Other nonradiative effects such as phonon-modulated Coulomb coupling with nearby impurities and thermal excitation to higher energy states,[39] and additional spectral diffusion from surface charge traps, might lead to a larger degree of nonradiative decay in nanodiamonds compared to bulk diamond. Typical optical coherence measurements of NV in nanodiamonds indicate that the nanodiamonds are a less ideal system than bulk diamond and contain more imperfections such as charge traps and dislocations than the bulk counterpart[52] (refer to Emission Rate Studies). To better quantify the influences of these possible imperfections and their contributions to the overall quantum efficiency, we now consider the case where the nonradiative decay rates are different in bulk and nanodiamonds. We can account for these effects by allowing the nonradiative component of the decay to increase in the nanodiamonds so that the bulk and nanodiamond quantum efficiencies are related as

$$\eta^{\text{nano}} = \frac{1}{1 - \gamma_i + 1/(\eta^{\text{bulk}}\beta_i)} \tag{6}$$

This equation is derived by introducing distinct nonradiative rates $\gamma_{\text{nr}}^{\text{bulk}}$ and $\gamma_{\text{nr}}^{\text{nano}}$. With the additional degree of freedom, the value of η^{nano} depends on the value chosen for η^{bulk}. The assumption of constant bulk NV quantum efficiency in eq 6 puts an additional constraint in the evaluation of the associated error. This results in lower error uncertainties (refer to Table 1) compared to those obtained using the quantum efficiency (eq 5).

If we have two sets of emission measurements of the same sample of nanodiamonds in different environments then η^{bulk} can be eliminated from eq 6, providing a direct measurement of the nanodiamond efficiency as

$$\eta^{\text{nano}} = \frac{\beta_1(1 - \gamma_1) - \beta_2(1 - \gamma_2)}{\beta_2\gamma_2 - \beta_1\gamma_1} \tag{7}$$

Unfortunately, in the present case of experiments with aerogel and glass coverslips, the contrast in the LDOS and therefore the radiative enhancement rates γ_i is relatively small, and the uncertainty limits that follow from eq 7 are too large for the obtained value for η^{nano} to be very informative. On the other hand, a higher contrast measurement using nanodiamonds in aerogel and nanodiamonds in a high index glass[54] or on a silicon substrate would certainly provide a meaningful result. Instead, here we obtain a value using eq 6 and inserting a value for the bulk quantum efficiency. Due to a lack of direct measurement of the bulk NV center value, we use the inferred value of 0.7 obtained in ref 9 to deduce the nanodiamond mean quantum efficiency (final column of Table 1). Again, these are mean values with errors that represent the uncertainty in the mean and not the width of the distribution of quantum efficiencies. It is evident that within our uncertainty the difference between nanodiamond and bulk diamond nonradiative contribution is not detectable. Another approach to measure the quantum efficiency could be based on the saturation curves obtained in different conditions.[11,55]

Quantum Efficiency Distribution. As already discussed, since we only have a statistical knowledge of the individual nanoenvironment of any center, and therefore of its radiative enhancement rate γ, our measurements and calculations provide estimates for the mean quantum efficiency and do not directly address the variation of quantum efficiencies across the sample. The error bounds in Table 1 should thus not be expected to encompass the range of possible quantum efficiencies across the sample. One might be tempted to estimate a width for the distribution of quantum efficiency by performing a simple Monte Carlo calculation of η using eq 5 with β_i and γ_i values drawn from the measured and calculated distributions of τ and γ. However, τ and γ are strongly correlated variables and treating them independently gives inappropriate results. In a very recent *arxiv* paper, Mohtashami and Koenderink[56] describe an elegant and careful "dynamic Drexhage" experiment in which a moving spherical mirror induces a change in the electromagnetic LDOS and allows an estimate of the quantum efficiency of individual NV centers. They find a large distribution in the NV quantum efficiencies related to the diamond crystal sizes. For single NV centers in 100 nm diamond crystals, they observed the quantum efficiency to be widely distributed between 10 and 90%, not inconsistent with the mean values we report here. However, for smaller crystals of size around 25 nm (smaller than most of our diamonds here), the quantum efficiency was found to be restricted to just 0−20%. As in the present work, however, they also cannot determine the dipole orientations and diamond shapes of their individual centers, which introduces unavoidable uncertainty in the quantum efficiency values.

CONCLUSIONS

In this paper, we investigated more closely the effects of the nanoenvironment on the radiative emission of nanodiamonds embedding NV centers by incorporating the nanodiamonds in an aerogel composite with a refractive index close to 1. This approach is used to separate the substrate influences on emission from other intrinsic phenomena occurring within

the nanodiamonds. In fact, we determined that an aerogel environment extends the average total lifetime of the defects and partially reduces the lifetime distribution. These changes arise due to the absence of a dielectric air/substrate (coverglass) interface near the emitting dipoles. Our simulations identified that the remaining lifetime distribution width could be attributed to the irregular geometry of the host nanodiamonds. Geometries with sharp edges (*i.e.*, cube or trapezoid) will give rise to sharp changes in the dipole electric field patterns nearby, resulting in a broader distribution. Therefore, correct radiative lifetime calculations should be performed considering the crystal geometry of the nanodiamonds. In addition, by comparing the total distribution of lifetimes obtained in two different environments, the aerogel and the coverslip, and using the radiative lifetime calculated by our FDTD approach, we obtained upper-bounds on the mean quantum efficiency for nanodiamond NV emitters.

Our estimated value of quantum efficiency for both coverslip and aerogel configurations is consistent within the error uncertainties with the previously reported value of 0.7.[9] This suggests that nonradiative effects are important in nanodiamonds and are also responsible for the broadening of the observed lifetime distribution. We also observed a lower quantum efficiency of the nanodiamonds on the coverslip compared to the aerogel environment, possibly suggesting an enhancement of nonradiative decay due to the substrate. Even if this result requires further investigations, it seems to agree with similar findings in other nanoprobes (*e.g.*, colloidal quantum dots), where the presence of additional nonradiative decays has been associated with substrate charge traps, ultimately linked to blinking of the nanoemitters.[57] In summary, this works clarifies and investigates to a deeper extent the radiative and nonradiative decay properties of NV centers in nanodiamonds by their incorporation in air-like environment and by suitable FDTD calculation. This enables a better understanding of the effect of the local nanoenvironment, corresponding to the highly dielectric nanodiamond host, on the emission properties of single NV centers. This work motivates additional studies using high-index substrates or surrounding material and adds relevant information for the deployment of nanodiamond NV centers in nanoscopy or as nanosensors.

MATERIALS AND METHODS

Aerogel Properties. Macroscopically, silica aerogels are lightweight, low density, and almost transparent pieces of glass.[27,29,30] However, most of the properties of aerogel are imparted from their microstructure: a convoluted network of interconnected thin glass strands, taking up only a small fraction (up to 10%) of the macroscopic volume of the sample. Visually, the subwavelength scale of the network causes Rayleigh-like scattering, giving aerogel samples a slight opalescent appearance, blue in scattering, and yellowish in transmission. The refractive index of aerogels is relatively independent of the microscopic structure. Since the structure is nanometer in scale, light samples many structural elements within a single wavelength and effectively averages the dielectric properties of the material. For a glass volume of ~5%, the effective refractive index is typically ~1.03−1.05, although it can be slightly adjusted by changes in the fabrication procedure. This is significantly lower than other apparently solid materials, making aerogel ideally suited to experiments where a low-index environment is required. The dimensions of the aerogel structure typically range from 1 to 5 nm for the glass elements and ~50 nm for the air-filled pores. Given the appropriate scale of these pores, various nanoparticles have been trapped as dopants.[44] Typically, this encapsulation is done during the wet-chemistry that is the start of the fabrication procedure. This means that many different materials can be easily incorporated into the aerogel network with a minimum of extra processing steps.

Sample Preparation. Aerogels were fabricated using the "two-step" process:[29] 1 mL of methanol containing 4×10^{-3} mol/L of ammonia (as catalyst) was mixed with 2 mL of tetramethoxysilane (TMOS) and 0.2 mL of water. After 15 min, 1 mL of the ammoniated methanol and 0.8 mL of water (the water containing 37.5 μg/mL of acid-cleaned (refer to Supporting Information) nanodiamonds) were added. This sol was poured into a polymethylmethacrylate (PMMA) cuvette, where after several more minutes it transformed into a wet-gel. The wet-gels were aged in a methanol bath for 2 weeks to allow the network time to strengthen, then bathed in 20% (by volume) hexamethyldisilazane (HMDS) in methanol to modify the surface of the silica network and make the resulting aerogel hydrophobic. The reaction byproducts, along with any excess HMDS, were then diffusively removed from the gel by immersion in a pure methanol bath for a further 2 days. The liquid methanol component was removed from the aged and treated wet-gels by supercritical drying in an autoclave. First, the methanol in the pores was diffusively exchanged with liquid carbon dioxide. Then, by increasing first the pressure and then the temperature, the liquid carbon dioxide was transformed to a supercritical fluid (80 bar, 31.1 °C). Finally, the carbon dioxide was slowly vented from the chamber until the pressure dropped to 1 bar. Despite the hydrophobic nature of the aerogel, the samples were removed from the autoclave and placed in a desiccated environment to prevent unnecessary ingress of moisture.

Lifetime and Photon Correlation Measurements. For both coverslip and aerogel samples, fluorescence from the NV centers was excited using a 100 mW continuous wave laser (Coherent Compass) operating at 532 nm, with ~200 μW power incident on the sample. The laser was focused through the back surface of the coverslip and onto the sample using a 100× infinity-corrected oil immersion objective lens with a numerical aperture of 1.3 (Olympus), and luminescence was collected confocally through a pinhole. A spectrometer (Acton) with a cooled CCD (Princeton Instruments) was used to characterize the luminescence, and a Hanbury Brown and Twiss (HBT) interferometer with single-photon-sensitive avalanche photodiodes (Perkin-Elmer SPCM-AQR-14) was used to measure the photon statistics. Photon counting and correlation was carried out using a time-correlated single-photon-counting (TCSPC) module (PicoHarp 300, PicoQuant GmbH).

Finite-Difference Time-Domain (FDTD) Emission Rate Calculations. We calculated the radiative decay rates of the nanodiamond NV centers on the coverslip or aerogel relative to the decay rate in bulk diamond using 3D finite-difference time-domain (FDTD) simulation.[48,49] For a given dipole position and orientation within the nanodiamond crystal, the electromagnetic field was excited by a sinusoidal point current source driven at a frequency $\nu = c/\lambda$ for $\lambda = 680$ nm, which is near the middle of the NV emission spectrum. The power P radiated by the dipole was calculated by integrating the time averaged Poynting flux

$\mathbf{S} = \langle \mathbf{E}(t) \times \mathbf{H}(t) \rangle$ over the surface of a cubic box enclosing the radiating dipole. The calculation was then repeated with the same dipole orientation in a uniform medium of index n_d = 2.416 to obtain the emitted power P_b corresponding to NV emission in bulk diamond. The radiative spontaneous emission rate relative to the rate in bulk diamond was then obtained as $\gamma_i = P_i/P_b$. The calculations were performed with a spatial grid of Δx = 1 nm, in a cubic domain of size 150 nm, which were found to give convergence to less than 2%. The Poynting flux integration was performed over a cubic box of 120 nm enclosing the dipole emitter. For each of the studied configurations, the distribution in lifetimes was constructed by performing 250 simulations with uniformly distributed random values of dipole position and orientation within the nanodiamond. To confirm the accuracy of our calculations, we checked that our simulation method reproduced the analytic results of Chew[37] for the spontaneous emission rate of a dipole inside a sphere emitting in air. The 1 nm numerical grid generated a lifetime distribution in close agreement with the analytic results with the mean lifetime accurate to 3% of the exact value γ^{-1}. This effect dominates the calculated radiative lifetimes for the coverslip and aerogel environments which are shown in Figure 4 in terms of the normalized radiative lifetime γ^{-1}.

Conflict of Interest: The authors declare no competing financial interest.

Acknowledgment. The work at Macquarie was produced with the assistance of the Australian Research Council under the ARC Center of Excellence Program (EQuS), Project Number CE110001013. Calculations for the work were performed using the NCI computational facility. F.I. thanks Debra Birch for TEM measurements performed at the Macquarie University Microscopy Unit. The work at Bath was funded by EPSRC grant EP/F018622/1 "Aerogels in fibre optics". T.B. thanks the Leverhulme Trust for a Research Fellowship.

Supporting Information Available: Procedures for acid cleaning of diamond crystals. This reduces the graphite contents and produces a dispersed solution of diamonds in water. This material is available free of charge *via* the Internet at http://pubs.acs.org.

REFERENCES AND NOTES

1. Scheel, S. Single-Photon Sources—An Introduction. *J. Mod. Opt.* **2009**, *56*, 141–160.
2. Michler, P.; Imamoglu, A.; Mason, M. D.; Carson, P. J.; Strouse, G. F.; Buratto, S. K. Quantum Correlation among Photons from a Single Quantum Dot at Room Temperature. *Nature* **2000**, *406*, 968–970.
3. Lounis, B.; Moerner, W. E. Single Photons on Demand from a Single Molecule at Room Temperature. *Nature* **2000**, *407*, 491–493.
4. Mizuochi, N.; Makino, T.; Kato, H.; Takeuchi, D.; Ogura, M.; Okushi, H.; Nothaft, M.; Neumann, P.; Gali, A.; Jelezko, F.; *et al.* Electrically Driven Single-Photon Source at Room Temperature in Diamond. *Nat. Photonics* **2012**, *6*, 299–303.
5. Aharonovich, I.; Castelletto, S.; Simpson, D. A.; Su, C.-H.; Greentree, A. D.; Prawer, S. Diamond-Based Single-Photon Emitters. *Rep. Prog. Phys.* **2011**, *74*, 076501.
6. Tisler, J.; Balasubramanian, G.; Naydenov, B.; Kolesov, R.; Grotz, B.; Reuter, R.; Boudou, J.-P.; Curmi, P. A.; Sennour, M.; Thorel, A.; *et al.* Fluorescence and Spin Properties of Defects in Single Digit Nanodiamonds. *ACS Nano* **2009**, *3*, 1959–1965.
7. Kurtsiefer, C.; Mayer, S.; Zarda, P.; Weinfurter, H. Stable Solid-State Source of Single Photons. *Phys. Rev. Lett.* **2000**, *85*, 290–293.
8. Gruber, A.; Drabenstedt, A.; Tietz, C.; Fleury, L.; Wrachtrup, J.; von Borczyskowski, C. Scanning Confocal Optical Microscopy and Magnetic Resonance on Single Defect Centers. *Science* **1997**, *276*, 2012–2014.
9. Rittweger, E.; Han, K. Y.; Irvine, S. E.; Eggeling, C.; Hell, S. W. STED Microscopy Reveals Crystal Colour Centres with Nanometric Resolution. *Nat. Photonics* **2009**, *3*, 144–147.
10. Waldherr, G.; Beck, J.; Steiner, M.; Neumann, P.; Gali, A.; Frauenheim, T.; Jelezko, F.; Wrachtrup, J. Dark States of Single Nitrogen-Vacancy Centers in Diamond Unraveled by Single Shot NMR. *Phys. Rev. Lett.* **2011**, *106*, 157601.
11. Schietinger, S.; Barth, M.; Aichele, T.; Benson, O. Plasmon-Enhanced Single Photon Emission from a Nanoassembled Metal-Diamond Hybrid Structure at Room Temperature. *Nano Lett.* **2009**, *9*, 1694–1698.
12. Hausmann, B. J. M.; Shields, B.; Quan, Q.; Maletinsky, P.; McCutcheon, M.; Choy, J. T.; Babinec, T. M.; Kubanek, A.; Yacoby, A.; Lukin, M. D.; *et al.* Integrated Diamond Networks for Quantum Nanophotonics. *Nano Lett.* **2012**, *12*, 1578–1582.
13. Park, Y.-S.; Cook, A. K.; Wang, H. Cavity QED with Diamond Nanocrystals and Silica Microspheres. *Nano Lett.* **2006**, *6*, 2075–2079.
14. Schietinger, S.; Benson, O. Coupling Single NV-Centres to High-Q Whispering Gallery Modes of a Preselected Frequency-Matched Microresonator. *J. Phys. B* **2009**, *42*, 114001.
15. Santori, C.; Barclay, P. E.; Fu, K.-M. C.; Beausoleil, R. G.; Spillane, S.; Fisch, M. Nanophotonics for Quantum Optics Using Nitrogen-Vacancy Centers in Diamond. *Nanotechnology* **2010**, *21*, 274008.
16. Stewart, L. A.; Zhai, Y.; Dawes, J. M.; Steel, M. J.; Rabeau, J. R.; Withford, M. J. Single Photon Emission from Diamond Nanocrystals in an Opal Photonic Crystal. *Opt. Express* **2009**, *17*, 18044–18053.
17. Wolters, J.; Schell, A. W.; Kewes, G.; Nusse, N.; Schoengen, M.; Doscher, H.; Hannappel, T.; Lochel, B.; Barth, M.; Benson, O. Enhancement of the Zero Phonon Line Emission from a Single Nitrogen Vacancy Center in a Nanodiamond *via* Coupling to a Photonic Crystal Cavity. *Appl. Phys. Lett.* **2010**, *97*, 141108.
18. van der Sar, T.; Hagemeier, J.; Pfaff, W.; Heeres, E. C.; Thon, S. M.; Kim, H.; Petroff, P. M.; Oosterkamp, T. H.; Bouwmeester, D.; Hanson, R. Deterministic Nanoassembly of a Coupled Quantum Emitter–Photonic Crystal Cavity System. *Appl. Phys. Lett.* **2011**, *98*, 193103.
19. Englund, D.; Shields, B.; Rivoire, K.; Hatami, F.; Vučkovic, J.; Park, H.; Lukin, M. D. Deterministic Coupling of a Single Nitrogen Vacancy Center to a Photonic Crystal Cavity. *Nano Lett.* **2010**, *10*, 3922–3926.
20. Choy, J. T.; Hausmann, B. J. M.; Babinec, T. M.; Bulu, I.; Khan, M.; Maletinsky, P.; Yacoby, A.; Loncar, M. Enhanced Single-Photon Emission from a Diamond-Silver Aperture. *Nat. Photonics* **2011**, *5*, 738–743.
21. Bulu, I.; Babinec, T.; Hausmann, B.; Choy, J. T.; Loncar, M. Plasmonic Resonators for Enhanced Diamond NV^- Center Single Photon Sources. *Opt. Express* **2011**, *19*, 5268–5276.
22. Brokmann, X.; Coolen, L.; Dahan, M.; Hermier, J. P. Measurement of the Radiative and Nonradiative Decay Rates of Single CdSe Nanocrystals through a Controlled Modification of Their Spontaneous Emission. *Phys. Rev. Lett.* **2004**, *93*, 107403.
23. Castelletto, S.; Aharonovich, I.; Gibson, B. C.; Johnson, B. C.; Prawer, S. Imaging and Quantum-Efficiency Measurement of Chromium Emitters in Diamond. *Phys. Rev. Lett.* **2010**, *105*, 217403.
24. Inam, F. A.; Gaebel, T.; Bradac, C.; Stewart, L.; Withford, M. J.; Dawes, J. M.; Rabeau, J. R.; Steel, M. J. Modification of Spontaneous Emission from Nanodiamond Colour Centres on a Structured Surface. *New J. Phys.* **2011**, *13*, 073012.
25. Greffet, J.; Hugonin, J.; Besbes, M.; Lai, N.; Treussart, F.; Roch, J. Diamond Particles as Nanoantennas for Nitrogen-Vacancy Color Centers. **2011**, arXiv:1107.0502G.
26. Geiselmann, M.; Juan, M.; Renger, J.; Say, J. M.; Brown, L. J.; Garcia de Abajo, F. J.; Koppens, F.; Quidant, R. 3D Optical Manipulation of a Single Electron Spin. *Nat. Nanotechnol.* **2013**, *8*, 175–179.
27. Pajonk, G. Transparent Silica Aerogels. *J. Non-Cryst. Solids* **1998**, *225*, 307–314.
28. Grogan, M. D. W.; Heck, S. C.; Hood, K. M.; Maier, S. A.; Birks, T. A. Structure of Plasmonic Aerogel and the Breakdown of

the Effective Medium Approximation. *Opt. Lett.* **2011**, *36*, 358–360.
29. Grogan, M.; Heck, S.; Xiao, L.; England, R.; Maier, S.; Birks, T. Control of Nanoparticle Aggregation in Aerogel Hosts. *J. Non-Cryst. Solids* **2012**, *358*, 241–245.
30. Pauzauskie, P. J.; Crowhurst, J. C.; Worsley, M. A.; Laurence, T. A.; Kilcoyne, A. L. D.; Wang, Y.; Willey, T. M.; Visbeck, K. S.; Fakra, S. C.; Evans, W. J.; *et al.* Synthesis and Characterization of a Nanocrystalline Diamond Aerogel. *Proc. Natl. Acad. Sci. U.S.A.* **2011**, 10.1073/pnas.1010600108.
31. Purcell, E. M. Spontaneous Emission Probabilities at Radio Frequencies. *Phys. Rev.* **1946**, *69*, 681.
32. Beveratos, A.; Brouri, R.; Gacoin, T.; Poizat, J.-P.; Grangier, P. Nonclassical Radiation from Diamond Nanocrystals. *Phys. Rev. A* **2001**, *64*, 061802.
33. Ruijgrok, P. V.; Wüest, R.; Rebane, A. A.; Renn, A.; Sandoghdar, V. Spontaneous Emission of a Nanoscopic Emitter in a Strongly Scattering Disordered Medium. *Opt. Express* **2010**, *18*, 6360–6365.
34. Beveratos, A.; Brouri, R.; Gacoin, T.; Villing, A.; Poizat, J. P.; Grangier, P. Single Photon Quantum Cryptography. *Phys. Rev. Lett.* **2002**, *89*, 187901.
35. Lukosz, W.; Kunz, R. E. Light Emission by Magnetic and Electric Dipoles Close to a Plane Dielectric Interface. II. Radiation Patterns of Perpendicular Oriented Dipoles. *J. Opt. Soc. Am.* **1977**, *67*, 1615–1619.
36. Kreiter, M.; Prummer, M.; Hecht, B.; Wild, U. P. Orientation Dependence of Fluorescence Lifetimes near an Interface. *J. Chem. Phys.* **2002**, *117*, 9430–9433.
37. Chew, H. Radiation and Lifetimes of Atoms Inside Dielectric Particles. *Phys. Rev. A* **1988**, *38*, 3410–3416.
38. Schniepp, H.; Sandoghdar, V. Spontaneous Emission of Europium Ions Embedded in Dielectric Nanospheres. *Phys. Rev. Lett.* **2002**, *89*, 257403.
39. Muller, T.; Aharonovich, I.; Wang, Z.; Yuan, X.; Castelletto, S.; Prawer, S.; Atature, M. Phonon-Induced Dephasing of Chromium Colour Centres in Diamond. *Phys. Rev. B* **2012**, *86*, 195210.
40. Prawer, S.; Nemanich, R. J. Raman Spectroscopy of Diamond and Doped Diamond. *Philos. Trans. R. Soc., A* **2004**, *362*, 2537–2565.
41. Smith, B. R.; Gruber, D.; Plakhotnik, T. The Effects of Surface Oxidation on Luminescence of Nano Diamonds. *Diamond Relat. Mater.* **2010**, *19*, 314–318.
42. Zhao, H.-Q.; Fujiwara, M.; Takeuchi, S. Suppression of Fluorescence Phonon Sideband from Nitrogen Vacancy Centers in Diamond Nanocrystals by Substrate Effect. *Opt. Express* **2012**, *20*, 15628–15635.
43. Fricke, J.; Reichenauer, G. Structural Investigaticn of SiO_2 Aerogels. *J. Non-Cryst. Solids* **1987**, *95−96*, 1135–1141.
44. Morris, C. A.; Anderson, M. L.; Stroud, R. M.; Merzbacher, C. I.; Rolison, D. R. Silica Sol as a Nanoglue: Flexible Synthesis of Composite Aerogels. *Science* **1999**, *284*, 622–624.
45. Bradac, C.; Gaebel, T.; Naidoo, N.; Rabeau, J. R.; Barnard, A. S. Prediction and Measurement of the Size-Dependent Stability of Fluorescence in Diamond over the Entire Nanoscale. *Nano Lett.* **2009**, *9*, 3555–3564.
46. Beha, K.; Batalov, A.; Manson, N. B.; Bratschitsch, R.; Leitenstorfer, A. Optimum Photoluminescence Excitation and Recharging Cycle of Single Nitrogen-Vacancy Centers in Ultrapure Diamond. *Phys. Rev. Lett.* **2012**, *109*, 097404.
47. Press, W. H.; Teukolsky, S. A.; Vetterling, W. T.; Flannery, B. P. Numerical Recipes: The Art of Scientific Computing. *Numerical Recipes: The Art of Scientific Computing*, 3rd ed.; Cambridge University Press: New York, 2007.
48. Xu, Y.; Vučković, J. S.; Lee, R. K.; Painter, O. J.; Scherer, A.; Yariv, A. Finite-Difference Time-Domain Calculation of Spontaneous Emission Lifetime in a Microcavity. *J. Opt. Soc. Am. B* **1999**, *16*, 465–474.
49. Koenderink, A. F.; Kafesaki, M.; Soukoulis, C. M.; Sandoghdar, V. Spontaneous Emission Rates of Dipoles in Photonic Crystal Membranes. *J. Opt. Soc. Am. B* **2006**, *23*, 1196–1206.
50. Rogobete, L.; Schniepp, H.; Sandoghdar, V.; Henkel, C. Spontaneous Emission in Nanoscopic Dielectric Particles. *Opt. Lett.* **2003**, *28*, 1736–1738.
51. Siyushev, P.; Pinto, H.; Gali, A.; Jelezko, F.; Wrachtrup, J. Low Temperature Studies of Charge Dynamics of Nitrogen-Vacancy Defect in Diamond. **2012**, arXiv:1204.4898S.
52. Wolters, J.; Sadzak, N.; Schell, A. W.; Schröder, T.; Benson, O. Measurement of the Ultrafast Spectral Diffusion of the Optical Transition of Nitrogen Vacancy Centers in Nano-Size Diamond Using Correlation Interferometry. *Phys. Rev. Lett.* **2013**, *110*, 027401.
53. Evaluation of Measurement Data—Guide to the Expression of Uncertainty in Measurement (GUM), 1st ed.; Joint Committee for Guides in Metrology, 2008.
54. Henderson, M. R.; Gibson, B. C.; Ebendorff-Heidepriem, H.; Kuan, K.; Afshar, V., S.; Orwa, J. O.; Aharonovich, I.; Tomljenovic-Hanic, S.; Greentree, A. D.; Prawer, S.; *et al.* Diamond in Tellurite Glass: A New Medium for Quantum Information. *Adv. Mater.* **2011**, *23*, 2806–2810.
55. Castelletto, S.; Boretti, A. Radiative and Nonradiative Decay Rates in Chromium-Related Centers in Nanodiamonds. *Opt. Lett.* **2011**, *36*, 4224–4226.
56. Mohtashami, A.; Femius Koenderink, A. Suitability of Nanodiamond NV Centers for Spontaneous Emission Control Experiments. *New J. Phys.* **2012**, arXiv:1212.5172.
57. Orrit, M. Single-Photon Sources: Frequency Jitter of a Nano-Emitter. *Nat. Photonics* **2010**, *4*, 667–668.